agriculture

Article

Research on Optimization of the Bulb Form of the Bulb Tubular Pump Device for a Low-Head Agricultural Irrigation Pumping Station

Hongyin Zhang [1], Jianlong Liu [2], Jinxin Wu [1], Weixuan Jiao [1,*], Li Cheng [1] and Mingbin Yuan [1]

[1] College of Hydraulic Science and Engineering, Yangzhou University, Yangzhou 225100, China; chengli@yzu.edu.cn (L.C.)
[2] Management Division of Qinhuai River Hydraulic Engineering of Jiangsu Province, Nanjing 210022, China
* Correspondence: jiaowx@yzu.edu.cn

Abstract: A bulb tubular pump unit is a horizontal tubular pump unit composed of a water pump and bulb with an electric motor installed. Electric motors, transmission equipment, and bearings are usually placed in the bulb. The bulb is located in the flow channel and has a relatively narrow space. Therefore, the shape of the bulb has a significant influence on the flow pattern and pump efficiency in the flow channel. In this study, the CFX 19.2 software was employed to optimize the bulb hydraulically according to its geometry and parameters. The research results indicate that the flow pattern at the tail of the elliptical bulb was better, the hydraulic loss at the bulb section was small, and the device efficiency was higher than that at the tail, which was round. The streamlined support had small flow resistance, minimal hydraulic loss, and a high pump unit head and efficiency. Nine schemes were selected, and the geometrical characteristics and parameters of the bulb were determined as follows: the shape of the tail of the bulb was oval, the bulb ratio was 0.96, and the shape of the support parts was streamlined. The results hold important reference significance to improve efficiency and broaden the operating conditions of bulb tubular pump devices.

Keywords: bulb tubular pump; bulb form; optimization design; numerical simulation; hydraulic performance

Citation: Zhang, H.; Liu, J.; Wu, J.; Jiao, W.; Cheng, L.; Yuan, M. Research on Optimization of the Bulb Form of the Bulb Tubular Pump Device for a Low-Head Agricultural Irrigation Pumping Station. *Agriculture* **2023**, *13*, 1698. https://doi.org/10.3390/agriculture13091698

Academic Editors: Redmond R. Shamshiri, Muhammad Sultan, Md Shamim Ahamed and Muhammad Farooq

Received: 11 August 2023
Revised: 22 August 2023
Accepted: 25 August 2023
Published: 28 August 2023

1. Introduction

Agricultural drought leads to a reduction in food production and is a serious natural disaster phenomenon. Water conservancy is an important piece of infrastructure of the national economy, and pumping stations are an important component of water conservancy projects, which are key to protecting and developing food production. In particular, large pumping stations bear the heavy responsibility of regional flood control, irrigation, water diversion, and water supply. The benefits of irrigation pumping stations are mainly reflected in the reduction in the effects agricultural drought [1,2]. By increasing water used for irrigation, agricultural drought is alleviated, and food production is guaranteed.

Low-head pump stations are the main type of pump stations in the middle and lower reaches of the Yangtze River and the Pearl River Deltas in China. Due to the low and flat terrain in these areas, low-head pumping stations are often used. The construction of low-head pumping stations has promoted the construction of agricultural production bases with stable and high yields in China, ensuring economic development and people's productivity and survival. The bulb tubular pump device is one of the main types of low-head pumping stations along the Yangtze River and is also an important component of high-efficiency irrigation systems. The bulb tubular pump device has the advantages of smooth inlet and outlet channels, low hydraulic loss, and high channel efficiency, making it the most reasonable device type in theory for large-flow and low-head pumping stations. This economical pump type combines the technical characteristics of a diving motor and through-flow pump. With the rapid development of water conservancy in China and the extensive implementation of water diversion projects, the use of submersible tubular pumps has been consistently increasing and fully applied, which has played a significant role in promoting the development of the national economy.

The pump device is the core component of the pumping station. At present, research on pump devices mainly focuses on hydraulic optimization [3–5] and hydraulic stability [6–8]. The research results provide a reference for the design and optimization of a bulb tubular pump device. Numerical simulation based on computational fluid dynamics (CFD) technology is the main method for hydraulic optimization research of pump devices [9–11]. Zhou et al. [12] adopted the RNG k–ε turbulence model and SIMPLEC algorithm, based on the multi-rotation coordinate system model, and calculated the steady flow of two typical forms of post-installed tubular pumps, as well as a traditional cylindrical bulb and a spin-cone slender bulb with a total length of 10.72 D (D is the impeller diameter), and obtained the overall flow field results. Zhang et al. [13] combined the working condition's regulation mode, transmission mode, and overall structure and found that bulb tubular pumps with different structures were safe and reliable. Sun et al. [14] used the method of combining numerical simulation and experimental testing to analyze the differences between the external and internal characteristics of the two schemes involving a front-mounted bulb and a rear-mounted bulb. This research can provide reference for the design and form selection of a submersible tubular pump device, which has great engineering significance. Although some experts have conducted some work on the hydraulic optimization of bulb tubular pump devices in the early stage, with the development of CFD technology and pump device theory, the original research cannot meet the current needs.

The hydraulic stability of the pump device is also an important factor affecting the efficiency of the pumping station [15–17]. Stall [18,19], cavitation [20,21], and inlet vortices [22,23] are unstable water phenomena that occur during the operation of the pump unit. At present, experts and scholars mainly conduct research on the formation mechanism and suppression measures of hydraulic instability in pump devices and have achieved certain research results, which can provide guidance for the safe and stable operation of pump stations.

To sum up, however, little research has been conducted on the shape of the bulb. Therefore, in this study, we used CFX 19.2 software to optimize the shape of the bulb, which holds important reference significance to improve efficiency and broaden the operating conditions of bulb tubular pump devices.

2. Numerical Simulation

2.1. Three-Dimensional Geometric Model

In this study, the single-unit design flow rate of the tubular pump was 64 m^3/S, the single power was 3550 kW, the speed was 85.7 r/min, the head size was 3.15 m, and the impeller diameter range D was 5.14 m. As shown in Figure 1, the bulb tubular pump device consists of components such as the inlet duct, impeller, guide vane, bulb body, and outlet duct. The bulb tubular pump device is a rear-mounted bulb tubular pump device, and the bulb body is placed in the outlet duct. Unlike other types of pumping stations, placing the bulb body inside the pump device will have an impact on the flow of water in the duct and increase hydraulic losses. Therefore, it is necessary to conduct research on the key structural parameters of the bulb body.

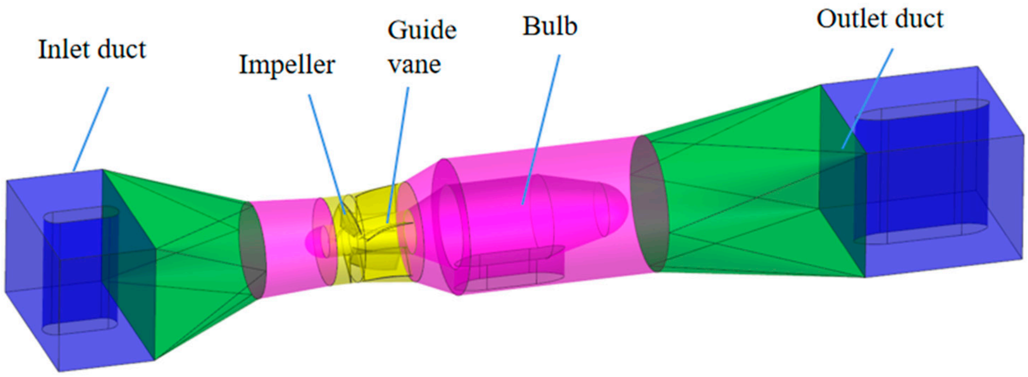

Figure 1. Schematic diagram of bulb tubular pump.

2.2. Numerical Simulation

2.2.1. Calculation Method

In order to ensure the accuracy of the calculation, this article divides the overall pump device into block grids as shown in Figure 2. ANSYS 19.2 Turbo Grid software was used for grid division of the impeller and guide vane calculation domain, and ANSYS 19.2 Mesh software was used for grid division of other areas. Hexahedral grids were used for each part of the grid to ensure the orthogonality and high quality of the calculation grid, and the grid quality of each part was above 0.85. At the same time, in order to accurately simulate the real situation, this paper conducts mesh refinement processing in various calculations and boundary layers. After this grid was partitioned into blocks, each block was output separately and then each part was merged during the CFX pretreatment to establish the interface area and solution conditions for calculation.

Figure 2. Mesh layout.

2.2.2. Computational Grid Independence Analysis

The quality and quantity of the grid have a significant influence on the accuracy and reliability of the numerical results. Turbo-Grid provides a self-checking function of grid quality, which generally makes the surface shape of the blades smooth and also generates better topology and grid quality. In terms of the number of grids, in theory, the more grids the model has, the smaller the solution error caused by the grid is. As the number of grids increases, so too does the requirement for computer configuration and calculation speed. Therefore, on the basis of ensuring the solution accuracy to a certain extent, the number of grids should not be too large. Before the numerical calculation, the number of grids should be analyzed to achieve the purpose of grid independence. Therefore, we conducted a grid independence analysis for a bulb tubular pump impeller (see Table 1).

Table 1. Number of impeller domain grids.

Grid	Impeller Grid/Million	Guide Vane Grid/Million	Passage Inlet Grid/Million	Passage Outlet (Including Bulb) Grid/Million	Total Grid/Million
1	1.40	1.80	2.60	3.00	8.80
2	1.50	1.80	2.60	3.00	8.90
3	1.60	1.80	2.60	3.00	9.00
4	1.70	1.80	2.60	3.00	9.10
5	1.80	1.80	2.60	3.00	9.20
6	1.90	1.80	2.60	3.00	9.30

A grid independence analysis was conducted according to the calculation formula of efficiency and head. The head H and the efficiency η of the bulb tubular pump device were used as the main evaluation indices. As the number of grids increased, the head and efficiency of the device decreased gradually. It is worth noting that the relative error between the fifth and sixth scheme is within 1%, and it can be considered that the number of grids has already met the independence requirement at this time, as shown in Figure 3.

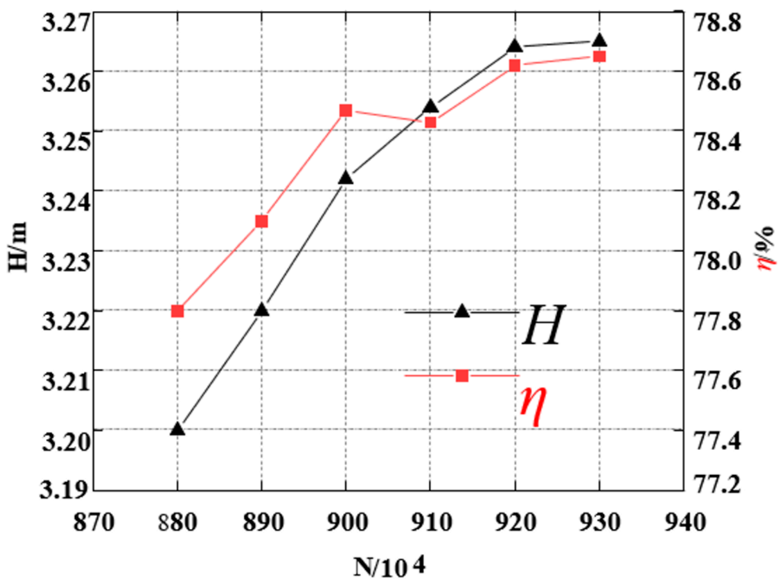

Figure 3. Grid independence analysis.

2.2.3. Calculation Parameters and Boundary Condition Setting

This paper uses the continuity equation based on incompressible fluid and the time-averaged Reynolds equation (RANS equation), and the SST k–ω model is used for the turbulence model. Hydraulic calculation based on the averaged Reynolds N-S equation is the prime method of numerical mathematics. Therefore, it is necessary to supplement the turbulence model to close the equation, and the selection of the turbulence model has a decisive influence on the accuracy of numerical simulation. Currently, the commonly used turbulence models include standard k–ε, SST k–ω, and others. Compared with the standard k–ε turbulence model, the SST k–ω turbulence model has the following advantages: the model can fully adapt to various physical phenomena, such as back pressure changes, and can be applied to the dense inner layer. The boundary layer phenomenon can be accurately simulated by applying the wall function without using the thick attenuation function, which is more easily distorted. Therefore, the SST k–ω turbulence model was applied to the numerical simulation of this pump device. The inlet of the device model was set as the mass flow inlet, which was initially set as 64,000 kg/s. The outlet was the average static pressure outlet, and the setting reference pressure was 1 atm. The interface was set to transfer the values between the components. The fixed wall was set as the nonslip boundary condition, the speed was initially set to 85.7 r/min, and the calculated residual control value was set to 10^{-4}.

2.2.4. Entropy Production Dissipation Theory

According to the second law of thermodynamics, the loss of mechanical energy is irreversibly converted into thermodynamic energy, a thermodynamic process that ultimately increases entropy production dissipation. In the interior of a pumping device, turbulent motion inevitably generates energy dissipation. Therefore, using the entropy production dissipation theory is appropriate to study the mechanism of hydraulic loss and energy dissipation inside the pumping device.

For turbulent flow, the entropy production dissipation based on the Reynolds time average can be divided into two parts: the viscous entropy production dissipation caused by fluid viscosity $\Delta S_{pro,\overline{D}}$ and the turbulent entropy production dissipation caused by turbulent pulsation $\Delta S_{pro,D'}$. In addition, the wall entropy production dissipation due to wall friction loss is $\Delta S_{pro,w}$.

The total entropy production dissipation of the whole device can be obtained from Equation (1) ΔS_{pro}.

$$\Delta S_{pro} = \Delta S_{pro,\overline{D}} + \Delta S_{pro,D'} + \Delta S_{pro,w} \tag{1}$$

The entropy production dissipation due to the time-averaged velocity can be calculated as follows:

$$\dot{S}'''_{\overline{D}} = \frac{\mu_{eff}}{T}\left\{2\left[\left(\frac{\partial\overline{u}}{\partial x}\right)^2 + \left(\frac{\partial\overline{v}}{\partial y}\right)^2 + \left(\frac{\partial\overline{w}}{\partial z}\right)^2\right] + \left[\left(\frac{\partial\overline{v}}{\partial x} + \frac{\partial\overline{u}}{\partial y}\right)^2 + \left(\frac{\partial\overline{w}}{\partial x} + \frac{\partial\overline{u}}{\partial z}\right)^2 + \left(\frac{\partial\overline{v}}{\partial z} + \frac{\partial\overline{w}}{\partial y}\right)^2\right]\right\} \tag{2}$$

where μ_{eff} is the dynamic viscosity (Pa-s) and $\overline{u}$, $\overline{v}$, and $\overline{w}$ are the time-averaged velocities in the direction of x, y, z components, (m/s).

The entropy production dissipation of turbulent dissipation due to velocity fluctuations can be calculated using the following Equation (3):

$$\dot{S}'''_{D'} = \beta\frac{\rho\omega k}{T} \tag{3}$$

where β = 0.09, ω is the turbulent eddy frequency (s^{-1}), and k is the turbulence energy (m^2/s^2).

The local entropy production dissipation integral of the computational domain is shown in Equations (4) and (5).

$$\Delta S_{pro,\overline{D}} = \int_V \dot{S}'''_{\overline{D}}\,\mathrm{d}V \tag{4}$$

$$\Delta S_{pro,D'} = \int_V \dot{S}'''_{D'}\,\mathrm{d}V \tag{5}$$

The wall entropy production dissipation can be calculated using the following equation:

$$\Delta S_{pro,w} = \int_A \frac{\vec{\tau}\cdot\vec{v}}{T}\,\mathrm{d}A \tag{6}$$

where $\vec{\tau}$ is the wall shear stress (Pa), A is the area (m^2), and $\underset{V}{\rightarrow}$ denotes the first grid velocity near the wall (m/s).

The analysis of energy loss in the bulb area of the pump device by means of entropy generation theory can intuitively show the size and distribution of energy dissipation in the pump device. Therefore, when optimizing the structure of the pump device, we can focus on the intensive area of entropy generation and dissipation in the pump.

3. Analysis of Calculation Results

3.1. Analysis on Influencing Factors of Hydraulic Performance of Bulb Section

Table 2 shows that the hydraulic loss of the bulb was the largest in the whole plant. Because the bulb was in the key position of the flow channel, it affected the flow pattern of water in the flow channel, thus greatly affecting the efficiency of the whole device [21]. Further analysis showed that under the designed flow condition, the hydraulic loss (except impeller) of the whole unit was the smallest; however, under the small-flow condition, the hydraulic loss was larger, and under the large-flow condition, the hydraulic loss was smaller than that under the small-flow condition. Under the condition of a large flow rate, the hydraulic loss also gradually increased with an increase in flow rate. The change rule of hydraulic loss of the bulb under different flow conditions was consistent with that of the whole plant. Therefore, an in-depth study on the bulb structure of the bulb tubular pump device would be helpful for a solid modeling and optimum design of the pump device.

Table 2. Proportion of hydraulic losses (%).

Flow Rate	Hydraulic Loss/M	Passage Inlet	Guide Vane	Bulb	Passage Outlet
$0.9Q_d$	0.663	3.66	43.06	39.30	13.98
$1.0Q_d$	0.258	15.43	28.29	35.43	20.85
$1.1Q_d$	0.343	9.89	25.73	42.42	21.96
$1.2Q_d$	0.484	5.95	28.97	47.43	17.65

Figures 4 and 5 respectively show the velocity streamline and velocity contour of the central axis of the bulb section. According to the diagram, under the condition of a small flow rate deviating from the design flow, the flow line at the rear of the bulb was chaotic and created a serious reflow phenomenon. As the flow rate increased, the reflow phenomenon at the rear of the bulb was significantly improved, and the flow line around the bulb was smoother. This result corresponded to the device efficiency values given in Table 3. At 1.2 times the design flow, the device efficiency value reached the highest level, which was 83.28%. Figure 4 shows a cloud image of the axial velocity distribution in the bulb segment. According to the diagram, under the small-flow condition, a large range of a low-speed zone appeared at the rear of the bulb and the front of the support. With an increase in flow, the range of the low-speed zone gradually decreased.

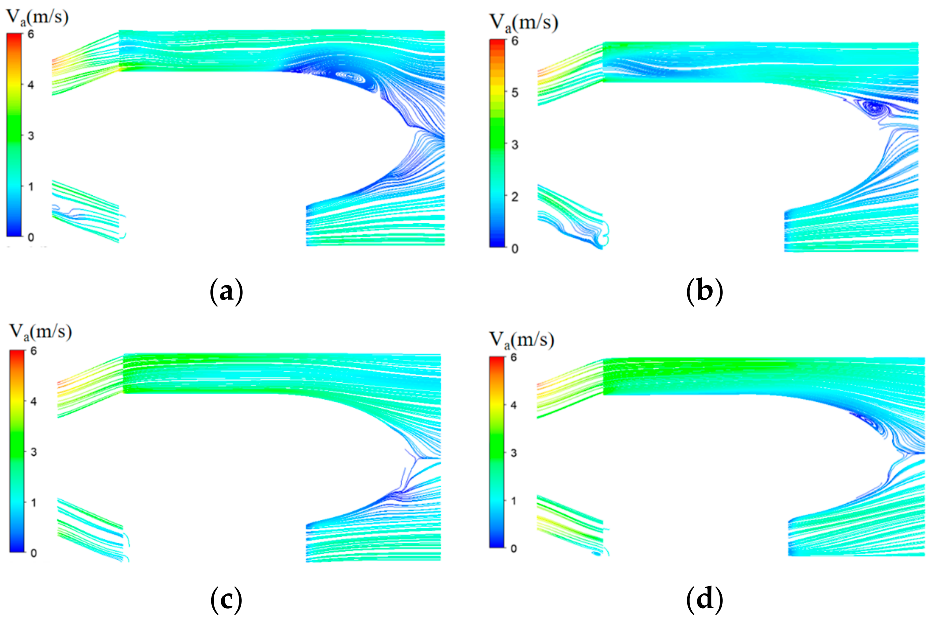

Figure 4. Streamline cloud diagram of axial velocity in bulb section: (**a**) $0.9Q_d$; (**b**) $1.0Q_d$; (**c**) $1.1Q_d$; (**d**) $1.2Q_d$.

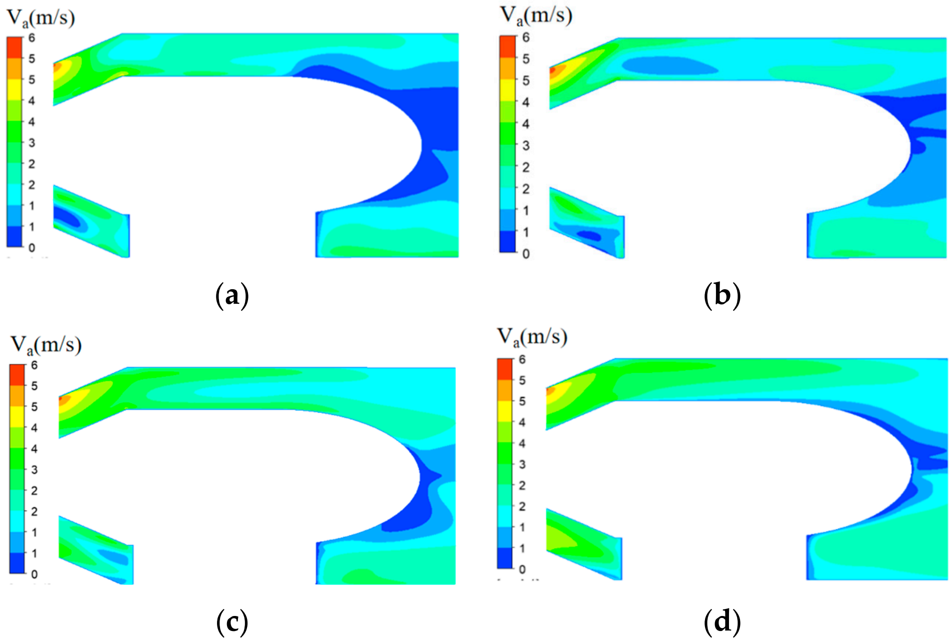

Figure 5. Contour image of axial velocity distribution in bulb section: (**a**) 0.9Q_d; (**b**) 1.0Q_d; (**c**) 1.1Q_d; (**d**) 1.2Q_d.

Table 3. Quantitative analysis of hydraulic performance of unit.

Flow	0.9Q_d	1.0Q_d	1.1Q_d	1.2Q_d
Head/m	3.56	3.27	2.89	2.38
Efficiency/%	73.87	78.75	82.17	83.28

3.2. Influence of Bulb Tail Shape on Hydraulic Performance

The shapes of the tail of the bulb studied were elongated, round, and oval (see Table 4). Different tail shapes have different effects on the flow pattern and thus on the performance of the whole device [19]. Therefore, in the design of the bulb structure, the shape of the tail of the bulb must be considered as an important research object.

Table 4. Research schemes 1–3.

Scheme	Bulb Tail Form	Three-Dimensional Model
1	First straight-line progressive section, then semi-ellipsoid; tail contraction angle is 27 degrees	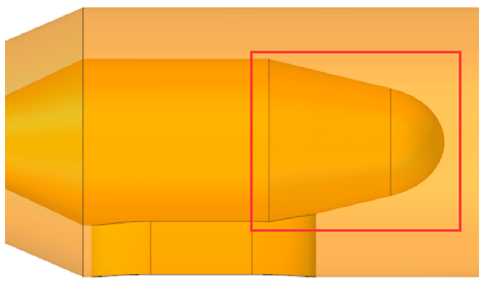

Table 4. *Cont.*

Scheme	Bulb Tail Form	Three-Dimensional Model
2	Hemisphere	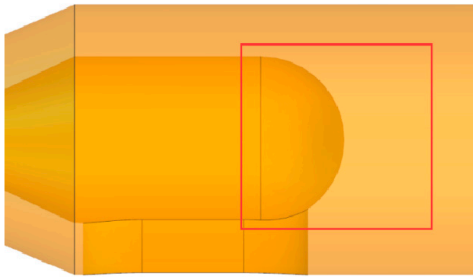
3	Semi-ellipsoid	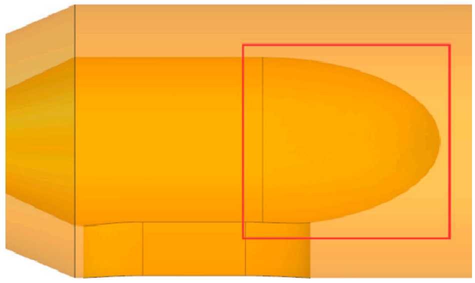

Figure 6 shows the head flow curve and the efficiency flow curve of the device with different bulb tail shapes. The diagram in scheme 3 clearly shows that the elliptical device at the tail of the bulb had a slightly higher efficiency than the other two schemes under the small flow rate from the highest efficiency point to the left. Under the condition of the high flow rate from the highest efficiency point to the right, the device efficiency was slightly lower than in scheme 1. Furthermore, the device head of scheme 3 was slightly higher than that of the other two schemes. This was due to the different shape and structure of the rear of the bulb and the different hydraulic losses of the bulb section. For the tail of the oval bulb, the low-speed range of the tail was reduced, the area where the vortex formed was smaller, and the water flow also followed a gradually diffusing trend. This result was more in line with the flow law of water flow, and its efficiency and head were improved.

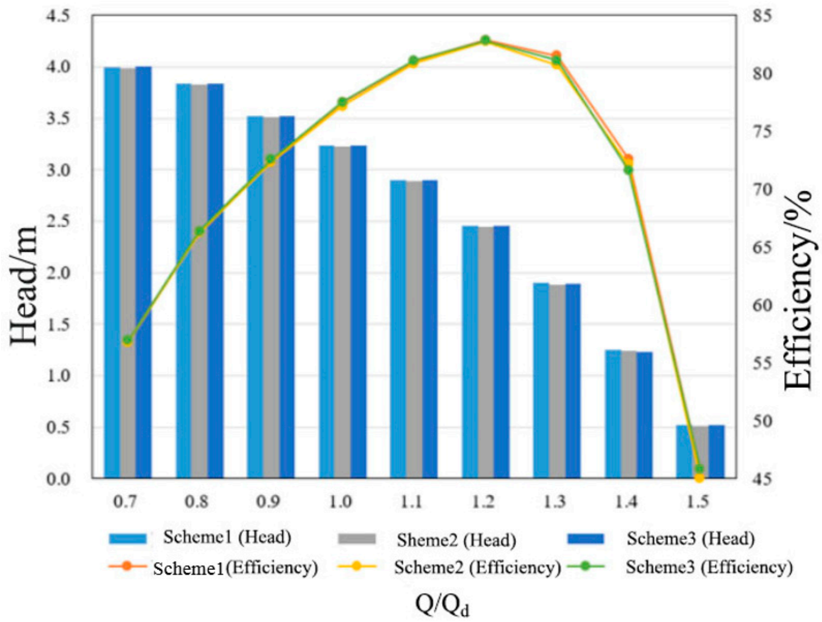

Figure 6. Device head flow curve and device efficiency flow curve with different bulb tail shapes.

Figure 7 shows the axial velocity streamline and velocity distributions in the bulb bodies with different tail shapes at design flow rate. As shown in the diagram, the tail back flow area of the bulb in scheme 2 was the largest, and the streamline was the most chaotic. In scheme 1, the streamline improved slightly because the tail of the bulb was extended slightly and the hydraulic loss in the bulb section was reduced. In scheme 3, the oval bulb tail body was used, and the water flow diffused smoothly. Therefore, the range of low-speed zone in the tail was the smallest, the area of vortex formation was the smallest, and the streamline was the smoothest.

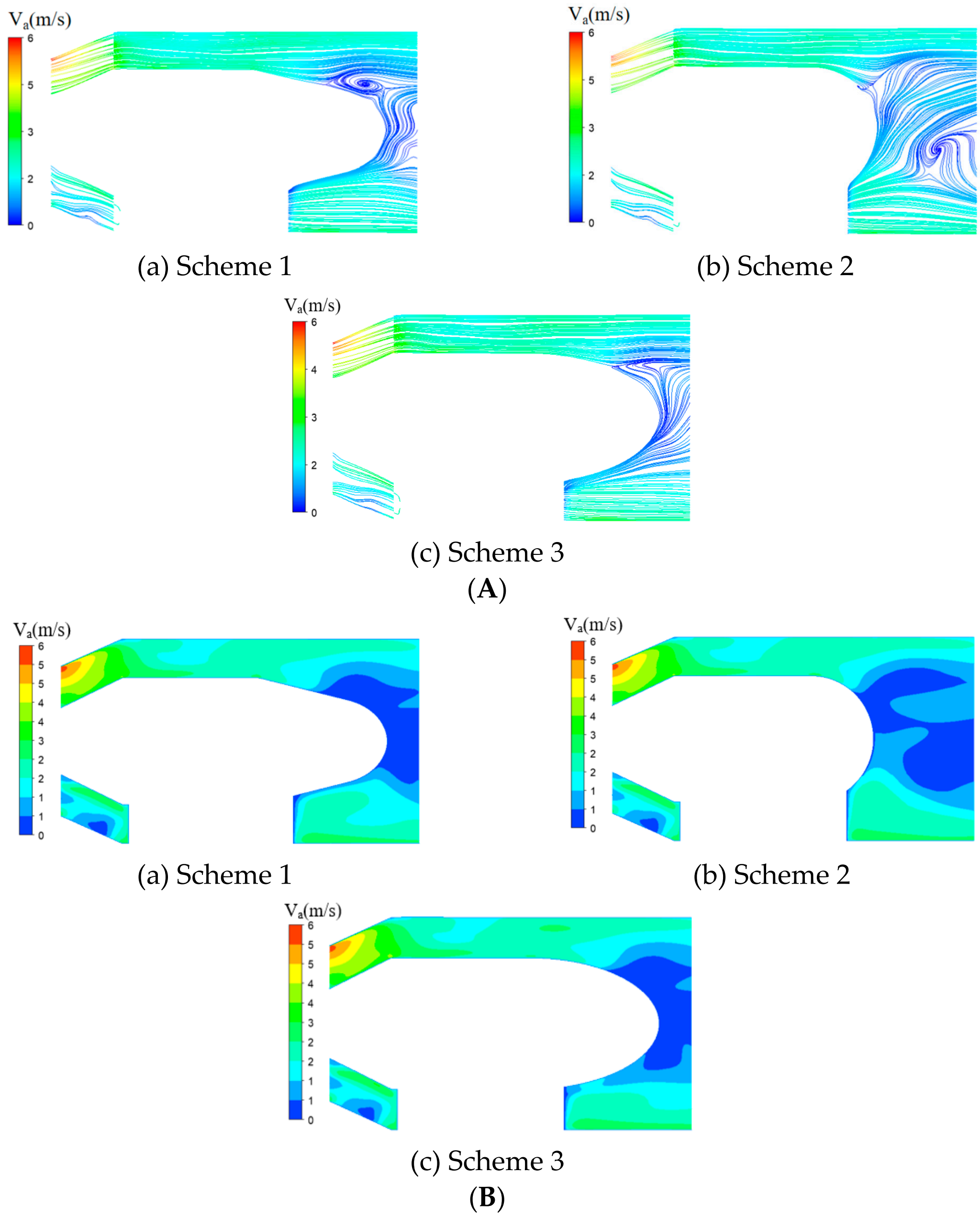

Figure 7. (**A**) Axial velocity streamline contour chart in the bulb bodies with different tail shapes at design flow rate; (**B**) Axial velocity contour chart in the bulb bodies with different tail shapes at design flow rate.

In order to further analyze the changes in pressure head caused by the changes in the structure of the bulb body, Figure 8 shows the static pressure contour chart at the outlet section of the bulb with different tail shapes. As shown in the diagram, the static pressure distribution at the outlet section of the bulb in scheme 3 was the most uniform, and the static pressure changed smoothly.

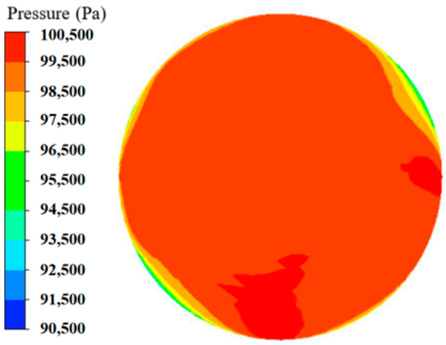

(**a**) Scheme 1

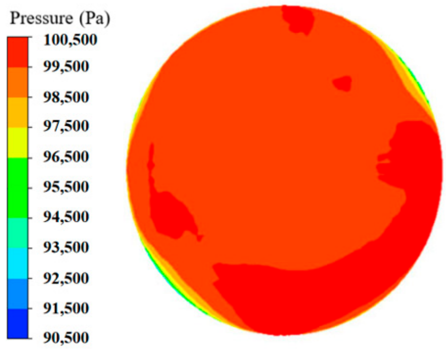

(**b**) Scheme 2

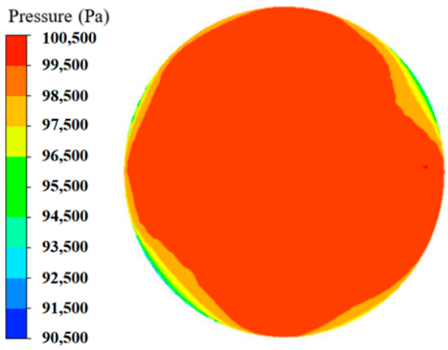

(**c**) Scheme 3

Figure 8. Static pressure contour chart.

The bulb structure in the rear-bulb tubular pump had a significant influence on hydraulic performance. In engineering design, it is recommended that the elliptical bulb body tail be used in the pumping station in combination with construction practice. To reduce the swirl area at the tail, the tail size of the bulb generally can be based on the total length of the bulb. Thus, the flow pattern distribution at the elliptical bulb body tail was improved to a certain extent by using the tail of the elliptical bulb. The hydraulic loss of the bulb section and the device performance also were improved compared with the round tail. For the pumping station, scheme 3 optimized the device and further reduced hydraulic losses by changing the bulb ratio.

3.3. Influence of Bulb Ratio on Hydraulic Performance

The bulb structure is used to place the electric motors and gearboxes in the tubular pump unit. The important dimension parameters are the bulb ratio and the ratio of the bulb diameter to the outer diameter of the impeller. The impeller diameter is generally a known parameter when designing the bulb section structure, whereas the bulb is determined according to its internal structure size, that is, according to the type and size of the motor and transmission equipment used in the device. Therefore, even in a pump unit with a same impeller, the bulb ratio can vary depending on the size and diameter of the bulb.

In practical design, the bulb diameter is usually expressed by the product of the bulb ratio and the impeller's outer diameter. The bulb diameter generally depends on the internal structural dimensions, such as the motor and transmission equipment. By referring to the data, we could determine when it would be necessary to use a small bulb and submerged asynchronous motor for the direct drive. The minimum bulb size could be arranged using a high-speed motor and gear box, and the bulb diameter was 0.76 D. When it was necessary to use the headlight body, according to the current manufacturing level of a high-voltage, high-speed motor and planetary gear reducer, it was reasonable to use a 0.9 D bulb diameter. If the synchronous motor was used in a direct connection, the diameter of the core was larger because the synchronous motor had to match the excitation system. Therefore, the diameter of the bulb should be more than 1.03 D. In the East Route Project of South-to-North Water Transfer, the bulb ratio of Jinhu Pump Station is 1.03 (i.e., the diameter of the bulb is 1.03 D). The bulb ratio of Linjiaba Pumping Station is 0.98 (i.e., the diameter of bulb is 0.98 D). The bulb ratio of Shandong Pumping Station with a water pump manufactured by the Japanese Yokogawa Company is 1.04 (i.e., the bulb diameter is 1.04 D) (Table 5).

Table 5. Research schemes 4–6.

Scheme	Bulb Ratio ($\frac{d_1}{D}$)	Three-Dimensional Diagram
4	0.88	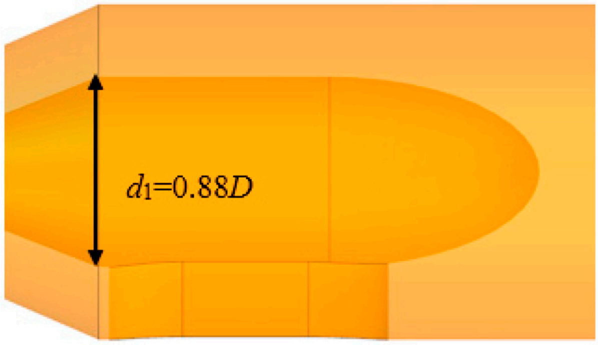
5	0.96	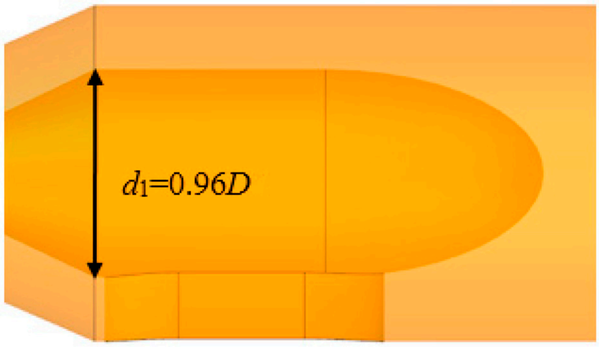
6	1.04	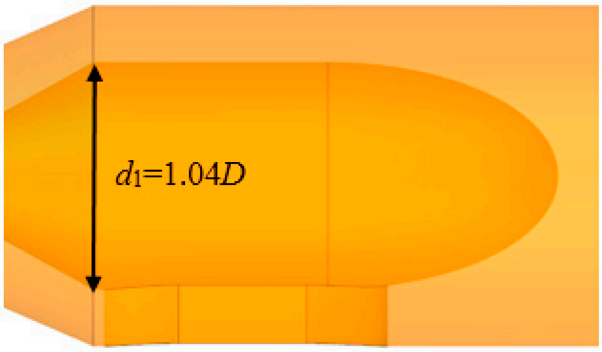

The device head curves and device efficiency curves for different bulb ratios are shown in Figure 9. According to this analysis, the device head was not affected by the change in the bulb ratio. The efficiency curves of the three bulb ratio schemes basically coincided with each other under the condition of a small flow rate from the highest efficiency point to the left, with little change. The device efficiency increased with the decrease in the bulb ratio under the condition of large flow to the right from the highest efficiency point, and the variation was obvious. This result was due to the small bulb ratio and the large flow area, creating a smoother flow pattern and higher efficiency in the bulb section.

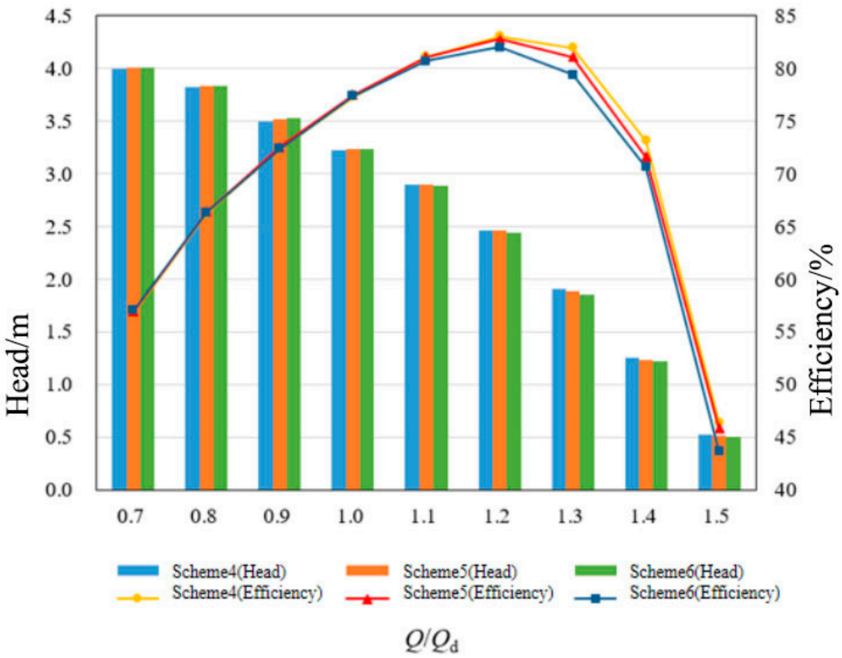

Figure 9. Head flow curve and efficiency flow curve of different bulb ratios.

The axial two-dimensional velocity streamline distributions in bulbs with different bulb ratios at the design flow rate are shown in Figure 10A. According to the diagram for scheme 6, the flow area of the bulb was reduced because of the large bulb ratio, the tail streamline was disordered, and the reflow phenomenon was serious. The tail streamlines of schemes 4 and 5 were relatively smooth. As shown in Figure 10B, we found that the loss of the entropy generation at the tail of scheme 6 was relatively large, whereas the loss of the entropy generation at the tails of schemes 4 and 5 had little change, which indicated that the hydraulic loss at the tail of the bulb of scheme 4 and 5 was small and the efficiency of the whole plant improved.

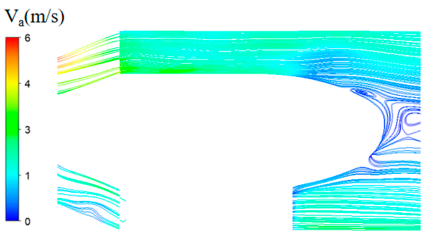

(a) Scheme 4

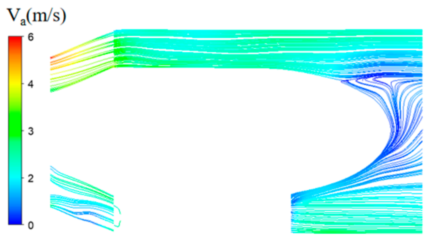

(b) Scheme 5

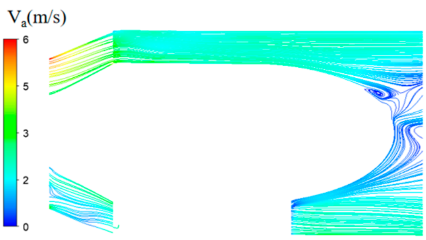

(c) Scheme 6

(**A**)

Figure 10. *Cont.*

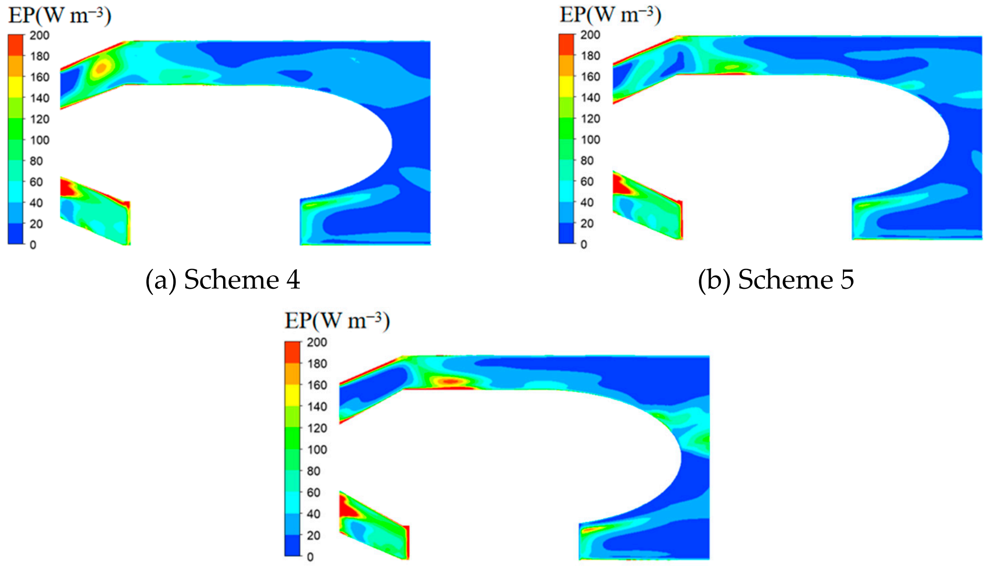

(a) Scheme 4 (b) Scheme 5

(c) Scheme 6

(**B**)

Figure 10. (**A**) Axial velocity streamline distribution in bulb bodies with different bulb ratios at design flow rate; (**B**) Axial surface entropic production distribution cloud in bulb bodies with different bulb ratios at design flow rate.

Schemes 4 and 5 had a small tail entropy output value, small hydraulic loss, and high efficiency. Considering that the pump station was directly connected by the synchronous motor, to facilitate the installation of the motor, we selected scheme 5 for optimization. By changing the shape of the support parts, the hydraulic loss of the bulb was further reduced, and the device efficiency was improved.

3.4. Influence of Support Shape on Hydraulic Performance

Bulb support is an important internal flow-passing part of the tubular pump unit. In this section, we used the CFD method to simulate the internal flow field of the bulb tubular pump unit and compared, analyzed, and optimized the shapes of the different supports. This provided a certain reference basis for the design and manufacture of the bulb tubular pump [20]. We used three schemes to compare the shapes of different bulb supports, as shown in Table 6. Among these supports, scheme 7 was the original support, and the support included one bottom support. In scheme 8, one bottom support in scheme 1 was divided into two parts, and the total width, length, and dimensions of the two supports remained unchanged. The distance between the two supports was 0.5 m. Scheme 9 streamlined the bottom support of the outer surface in scheme 1.

Figure 11 shows the flow head curve and flow efficiency curve of the bulb tubular pump unit for three schemes. From the flow efficiency curve, the differences among the three schemes were obvious. The efficiency of the pump unit of scheme 7 was about 0.4% higher than that of scheme 8 and that of scheme 9 was about 0.8% higher than that of scheme 8 at design flow rate, which indicated that the hydraulic loss caused by bulb support of tubular pump had a more significant influence on the hydraulic performance of the pump unit. From the flow head curve, the performance of scheme 7 was better than that of scheme 8, and scheme 9 was better than that of scheme 7, with a difference of about 0.4%. This result showed that different supports had an influence on the unit head, and this trend was consistent with hydraulic loss. The improved support structure in scheme 7 reduced the wet circumference of water flow and thus the friction loss of water. The shape of the streamlined support in scheme 9 followed the principle of minimum resistance of fluid movement, and the flow resistance of water flow was the smallest. Thus, the hydraulic loss was the smallest, and the pump unit head and efficiency were high.

Table 6. Research schemes 7–9.

Scheme	Support Shape	Three-Dimensional Model
7	Original scheme	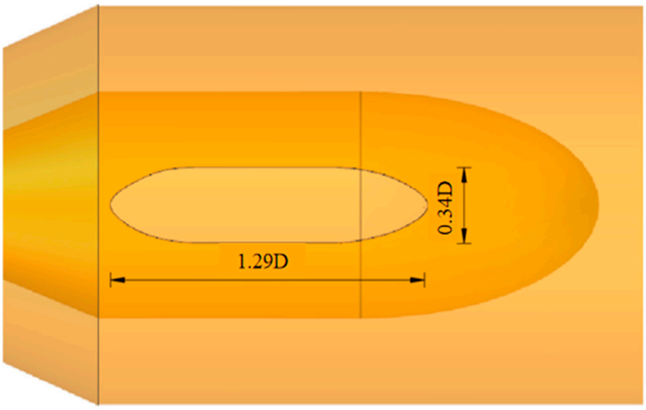
8	Split into two supports	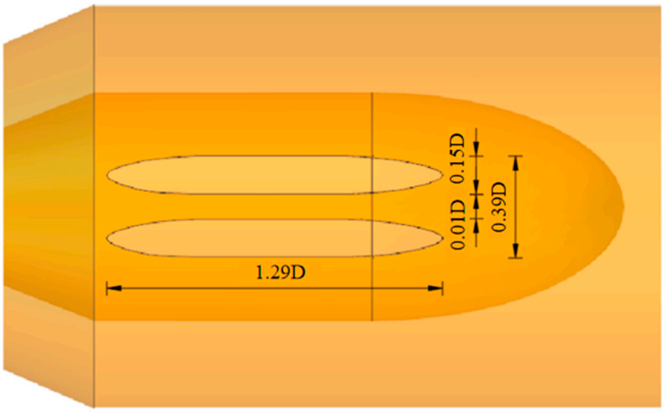
9	Streamline design	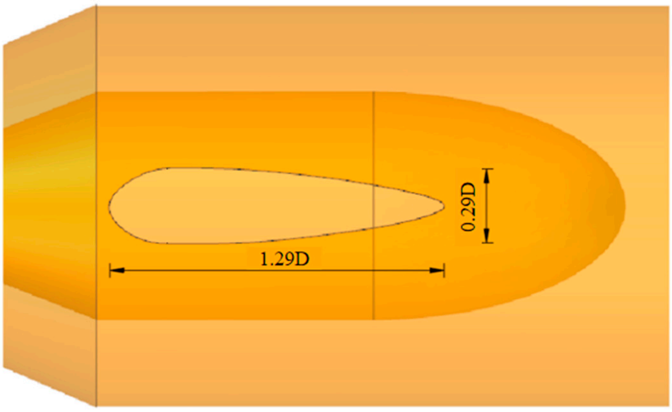

In Scheme 8, the support consisted of two bottom supports for the bulb. Because of the small distance between the two supports, there was little water flowing through this area, making it a dead-water zone. As shown in Figure 12, the water flow behind the support and the tail of the bulb was disordered, and the flow pattern was poor. The tail of the bulb also had a low-speed zone and a small range of back flow. In scheme 7, because the bottom support was combined into one, the flow area was increased and the flow resistance was reduced. As a result, the low-speed area and the return area at the rear of the bulb were significantly reduced. In scheme 9, the bottom support was changed into a streamlined one. The calculation results showed that the original undesirable flow pattern was significantly improved and the flow was relatively smooth, which was beneficial to further improve the efficiency of the pump unit.

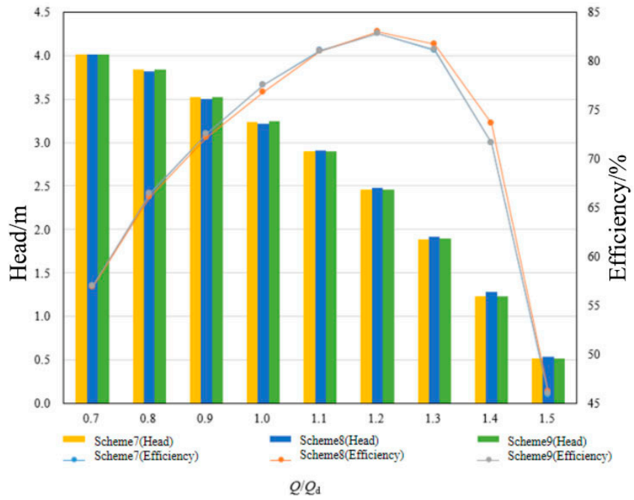

Figure 11. Head flow curve and device efficiency flow curve of different bulb support shapes.

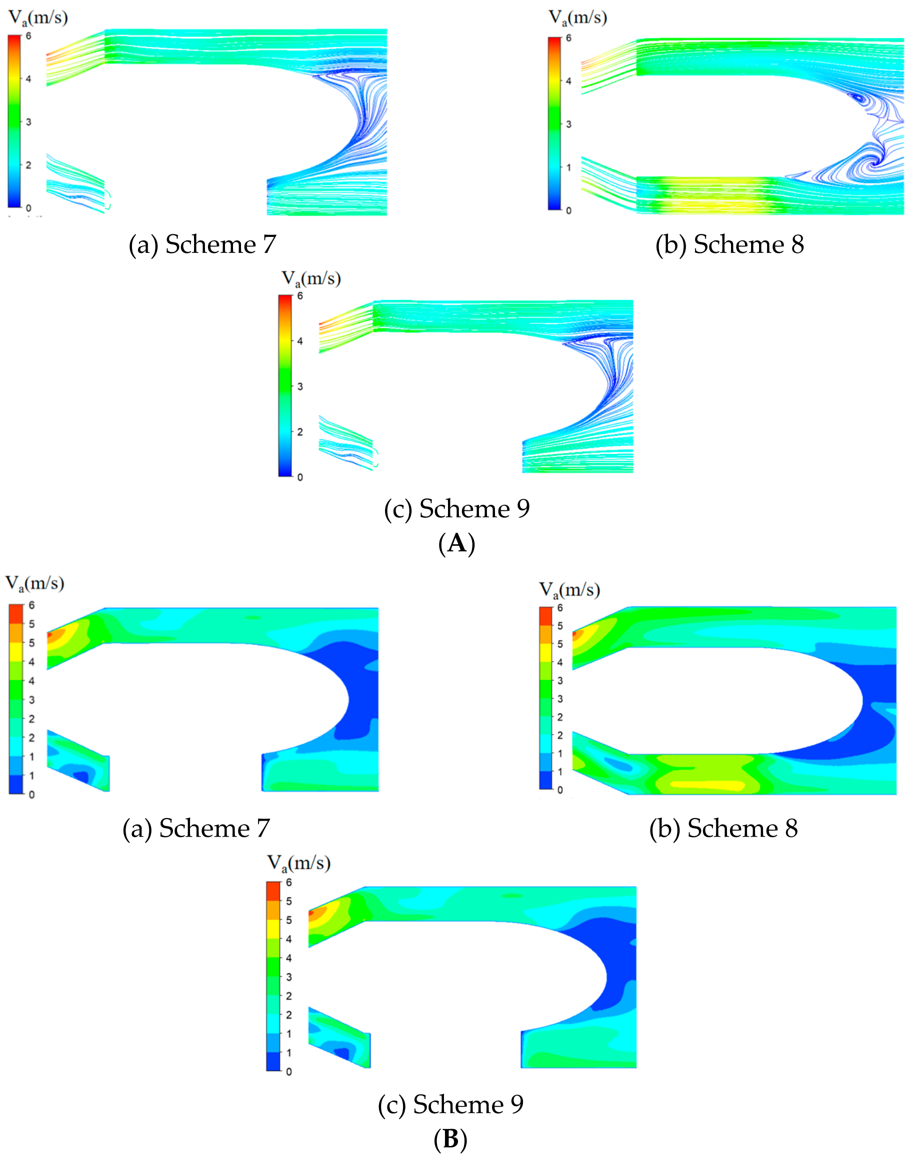

Figure 12. (**A**) Axial velocity streamline contour chart in the bulb bodies with different bulb support shapes at design flow rate; (**B**) Axial velocity contour chart in the bulb bodies with different bulb support shapes at design flow rate.

The variations in the hydraulic loss of the bulb section with flow rate under different schemes are shown in Figure 13. The hydraulic loss corresponding to the high-efficiency point was the smallest, and the hydraulic loss on the left side deviating from the high-efficiency point increased with a decrease in the flow rate. The hydraulic loss on the right side of the high-efficiency point increased with an increase in the flow rate. The increase in hydraulic loss in the small-flow area was mainly due to the increase in the pump outlet circulation caused by secondary back flow in the pump, which led to an increase in loss in the bulb. We found that merging the bottom supports reduced the hydraulic loss of the bulb section, and the water loss was also reduced after streamlining, thus improving the device efficiency.

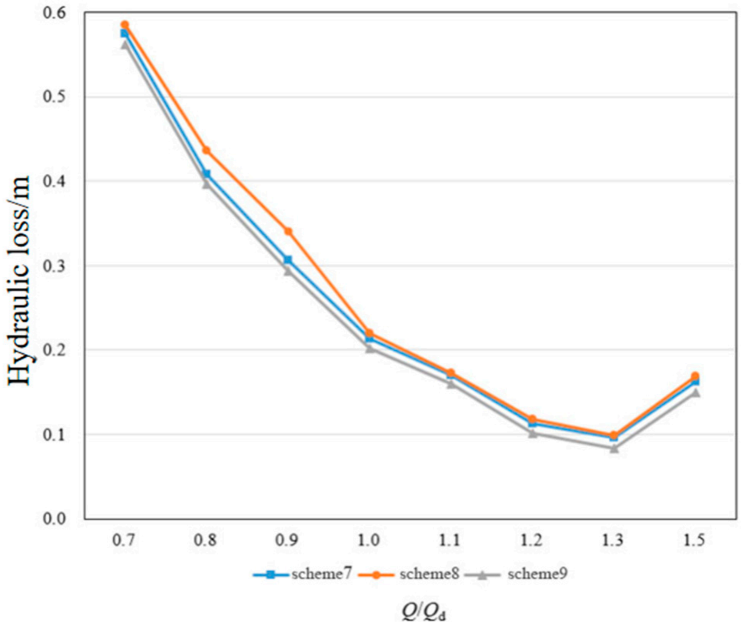

Figure 13. Hydraulic loss curve of bulb section.

In conclusion, the shape of the bottom support had a clear influence on the hydraulic loss and flow pattern of the pump unit. A reasonable shape of the support could improve the flow pattern, reduce water circulation, and improve the efficiency of the pump unit. Scheme 9's supports had better hydraulic performance, improved device efficiency, and achieved the purpose of optimization. Therefore, we selected scheme 9 as the bulb optimization scheme. Its geometric characteristics and parameters were as follows: the shape of the bulb tail was oval, the bulb ratio was 0.96, and the shape of the supports was streamlined.

4. Conclusions

In this study, the CFX 19.2 software was used to hydraulically optimize the bulb in accordance with the geometry and parameters. Through the calculation analysis and scheme comparison, we drew the optimized scheme of the bulb section. The conclusions are as follows:

(1) Because the bulb was in the key position of the flow channel, it affected the flow state in the flow channel and had a significant influence on the efficiency of the entire device. The hydraulic loss of the bulb part is about 40% of the overall hydraulic loss of the pump device, which accounts for the largest proportion of the entire pump device.

(2) Different tail shapes of the bulb had different effects on the flow pattern and the performance of the entire device. The flow pattern distribution at the tail of the bulb was improved to a certain extent by using the elliptical bulb tail. This reduces the

hydraulic loss of the bulb section and increases the efficiency of the device by about 5% compared to the hemisphere bulb structure.

(3) The bulb ratio of the bulb with a semi-ellipsoid tail shape was small, the flow area was large, the flow pattern was smoother, and the bulb section had higher efficiency. Schemes 4 and 5 had a small tail entropy output value, small hydraulic loss, and high efficiency. Considering that the pump station was directly connected by the synchronous motor, we selected scheme 5 to facilitate the installation of the motor.

(4) The bulb support is an important internal flow component of the tubular pump unit. A change in its shape had a significant influence on the flow pattern of the water in the pump unit and also on the hydraulic performance of the pump unit. Reasonable shape design of the support parts according to minimum resistance requirements effectively improved the flow pattern, reduced hydraulic losses, and improved the efficiency of the pump unit. Scheme 9's supports had better hydraulic performance, improved the device efficiency, and achieved the optimization purpose. Therefore, we selected scheme 9 as the bulb optimization scheme. Its geometric characteristics and parameters were as follows: the shape of the bulb tail was oval, the bulb ratio was 0.96, and the shape of the supports was streamlined.

Author Contributions: Software, W.J., H.Z. and J.W.; Validation, L.C. and W.J.; Writing—original draft, H.Z., M.Y. and J.W.; Formal analysis, H.Z. and J.W.; Writing—review and editing, W.J., J.L. and L.C.; Methodology, J.L. and L.C.; Supervision, W.J., L.C. and J.L. All authors have read and agreed to the published version of the manuscript.

Funding: This research was funded by the National Natural Science Foundation of China (grant no. 52279091), the Project Funded by the Priority Academic Program Development of Jiangsu Higher Education Institutions (PAPD), the Key Project of Water Conservancy in Jiangsu Province (Grant No: 2022017, 2022055), the Natural Science Foundation of the Jiangsu Higher Education Institutions of China (Grant No:23KJB570003), the Jiangsu Province College Students' Innovation and Entrepreneurship Training Program (202311117041Z), and the Open Project Program of Engineering Research Center of High-efficiency and Energy-saving Large Axial Flow Pumping device, Jiangsu Province, Yangzhou University (Grant No:ECHEAP025).

Institutional Review Board Statement: Not applicable.

Data Availability Statement: Data on the analysis and reporting results during the study can be obtained by contacting the authors.

Conflicts of Interest: The authors declare no conflict of interest.

References

1. Li, W.; Huang, Y.; Ji, L.; Ma, L.; Agarwal, R.K.; Awais, M. Prediction model for energy conversion characteristics during transient processes in a mixed-flow pump. *Energy* **2023**, *271*, 127082. [CrossRef]
2. Jiao, W.; Chen, H.; Cheng, L.; Zhang, B.; Gu, Y. Energy loss and pressure fluctuation characteristics of coastal two-way channel pumping stations under the ultra-low head condition. *Energy* **2023**, *278*, 127953. [CrossRef]
3. Sun, L.; Pan, Q.; Zhang, D.; Zhao, R.; van Esch, B.B. Numerical study of the energy loss in the bulb tubular pump system focusing on the off-design conditions based on combined energy analysis methods. *Energy* **2022**, *258*, 124794. [CrossRef]
4. Zhang, B.; Cheng, L.; Jiao, W.; Zhang, D. Experimental and statistical analysis of the flap gate energy loss and pressure fluctuation spatiotemporal characteristics of a mixed-flow pump device. *Energy* **2023**, *272*, 127117. [CrossRef]
5. Jia, X.; Lv, H.; Zhu, Z. Research on the influence of impeller tip clearance on the internal flow loss of axial circulating pump under unpowered driven condition. *ASME J. Fluids Eng.* **2023**, *145*, 021202. [CrossRef]
6. Zhang, B.; Yang, A.; Cheng, L.; Jiao, W.; Chen, Y.; Zhao, H. Spatial-temporal evolution and pressure fluctuation characteristics of the combined submerged vortex in a closed pump sump. *Phys. Fluids* **2023**, *35*, 065140.
7. Jiao, W.; Chen, H.; Cheng, L.; Zhang, B.; Yang, Y.; Luo, C. Experimental study on flow evolution and pressure fluctuation characteristics of the underwater suction vortex of water jet propulsion pump unit in shallow water. *Ocean. Eng.* **2022**, *266*, 112569. [CrossRef]
8. Song, X.J.; Luo, Y.Y.; Wang, Z.W. Numerical prediction of the influence of free surface vortex air- entrainment on pump unit performance. *Ocean. Eng.* **2022**, *256*, 111503. [CrossRef]
9. Pan, Q.; Shi, W.; Zhang, D.; Van Esch, B.P. Analysis, Design, and Validation of a Vaned Diffuser for Improved Fish Friendliness. *ASME J. Fluids Eng.* **2022**, *144*, 051502. [CrossRef]

10. Jiao, W.; Li, Z.; Cheng, L.; Wang, Y.; Zhang, B. Study on the Hydraulic and Energy Loss Characteristics of the Agricultural Pumping Station Caused by Hydraulic Structures. *Agriculture* **2022**, *12*, 1770. [CrossRef]
11. Ji, L.; Li, W.; Shi, W.; Tian, F.; Agarwal, R. Effect of Blade Thickness on Rotating Stall of Mixed-Flow Pump Using Entropy Generation Analysis. *Energy* **2021**, *236*, 121381. [CrossRef]
12. Zhou, J.R.; Cheng, L.; Liu, C.; Tang, F.P. Numerical simulation of bulb form of rear bulb penetration device. *J. Disch. Irrig. Mech. Eng.* **2011**, *29*, 72–76.
13. Zhang, R.T.; Shan, H.C.; Bu, G.; Zhou, W.; Zhu, H.G.; Yao, L.B. Structural characteristics of bulb tubular pump for Phase I project of East Route of South-to-North Water Transfer. *J. Drain. Irrig. Mech. Eng.* **2016**, *34*, 774–782+789.
14. Sun, Z.; Yu, J.; Tang, F. The Influence of Bulb Position on Hydraulic Performance of Submersible Tubular Pump Device. *J. Mar. Sci. Eng.* **2021**, *9*, 831. [CrossRef]
15. Wang, Z.; Zheng, Y.; Wang, F.; Lin, Z.; Huan, C.; Li, Y. Experimental Study on Energy Consumption and Hydraulic Stability for Distributed Pumping System. *Arab. J. Sci. Eng.* **2014**, *39*, 6883–6894. [CrossRef]
16. Zhang, X.; Tang, F.; Jiang, Y. Experimental and numerical study of reverse power generation in coastal axial flow pump system using coastal water. *Ocean. Eng.* **2023**, *271*, 113805. [CrossRef]
17. Liu, A.; Zhang, C.; Zhang, Y.; Zhang, Y. Analysis of hydraulic characteristics of fluid multiplier fish pump based on CFD simulation. *Ocean. Eng.* **2023**, *272*, 113854. [CrossRef]
18. Yang, Y.; Chen, X.; Bai, L.; Yao, Y.; Wang, H.; Ji, L.; He, Z.; Song, X.; Zhou, L. Quantification and investigation of pressure fluctuation intensity in a multistage electric submersible pump. *Phys. Fluids* **2023**, *35*, 035122. [CrossRef]
19. Yang, Y.; Li, W.; Shi, W.; Ping, Y.; Yang, Y.; Wang, L. Numerical investigation on the unstable flow at off-design condition in a mixed-flow pump. *Proc. Inst. Mech. Eng. Part A J. Power Energy* **2019**, *233*, 849–865. [CrossRef]
20. Huang, R.; Wang, Y.; Du, T.; Luo, X.; Zhang, W.; Dai, Y. Mechanism analyses of the unsteady vortical cavitation behaviors for a waterjet pump in a non-uniform inflow. *Ocean. Eng.* **2021**, *233*, 108798. [CrossRef]
21. Yang, Y.; Zhou, L.; Bai, L.; Xu, H.; Lv, W.; Shi, W.; Wang, H. Numerical Investigation of Tip Clearance Effects on the Performance and Flow Pattern within a Sewage Pump. *J. Fluids Eng. Trans. ASME* **2022**, *144*, 081202.
22. Jiao, W.; Zhao, H.; Cheng, L.; Yang, Y.; Li, Z.; Wang, C. Nonlinear dynamic characteristics of suction-vortex-induced pressure fluctuations based on chaos theory for a water jet pump unit. *Ocean. Eng.* **2023**, *268*, 113429.
23. Song, X.J.; Liu, C. Experiment study of the floor-attached vortices in pump sump using V3V. *Renew. Energy* **2021**, *164*, 752–766. [CrossRef]